Finite Element Analysis of a Deep Excavation supported using a Secant Pile Wall: A Case Study

V.S.S.D. Silva
Department of Civil Engineering
University of Moratuwa
Colombo, Sri Lanka
sachindeelakasilva@gmail.com

L.I.N. de Silva
Department of Civil Engineering
University of Moratuwa
Colombo, Sri Lanka
nalinds@uom.lk

2023 Moratuwa Engineering Research Conference (MERCon) | 979-8-3503-4521-6/23/$31.00 ©2023 IEEE | DOI: 10.1109/MERCon60487.2023.10355502

***Abstract*— Accurate finite element modeling (FEM) of deep excavations is a difficult task due to the lack of availability of details about the soil strata below ground level. This study proposes a method to select the appropriate parameters and correct modeling procedures in the FEM of deep excavation using measured field test data using two-dimensional analysis. Some studies indicate that the elastic modulus (E_{50}) of soil can be increased by several times to obtain the unloading-reloading modulus (E_{ur}) of the soil. The back analysis technique was used to calibrate the elastic modulus of the soil by comparing the lateral wall deformation profile obtained from the FEM analysis with the inclinometer readings acquired from the excavation site. The numerical model was validated using the behavior of a retaining wall at various excavation depths and analyzed through numerical simulations. Prop forces obtained from the numerical analysis were compared with those obtained from different empirical methods commonly used to estimate prop forces on multi-propped retaining structures. The study highlights that the elastic modulus of the soil can be increased between 2 and 4 times to obtain the unloading-reloading modulus of the soil.**

Keywords—Deep excavation, Finite element analysis, Elastic modulus, Back analysis

I. INTRODUCTION

Construction projects that involve deep excavation work have become a common feature in urban areas due to the growing scarcity of land in the world. Deep excavations are performed to construct basements, underground transportation systems, and water distribution networks. The retaining structures are constructed before conducting deep excavation work to avoid excessive horizontal and vertical ground movement, which can cause severe damage to the surrounding structures. Diaphragm walls, contiguous bored pile walls, and secant pile walls are the most commonly used earth retaining structures in deep excavation.

Struts are installed during deep excavation to support the retaining structure. Initially, the wall behaves as a cantilever, and after the installation of struts, it begins to act as a propped cantilever [1]. Ou [2] has classified the above two behaviors as cantilever type and braced excavation type. The wall displacement caused by deep excavation depends on many factors, such as soil condition, ground condition, surcharge load, construction method, groundwater level, strut spacing and stiffness, and retaining wall stiffness [3]. Accurate estimation of wall deformation during the design stage is complex due to the lack of detail in the soil strata below ground level. To reduce the risk, designers have used conservative design approaches.

A logical procedure to calculate the earth pressure acting on the retaining walls was first introduced by [4]. The limit-equilibrium method was used in that approach. Rankine [5] improved the previous work and introduced Rankine theory. This mathematical model provides a solution for the distribution of stresses within a soil mass to calculate active and passive earth pressures. Currently, several techniques are used to calculate prop forces acting on the support system in deep excavation work. Reference [6] has classified them as empirical, limit equilibrium, finite element, and other soil-structure interaction methods. Limit-equilibrium methods can only be used for cantilever and single-propped walls, as they are statically determinate problems. Free earth support, fixed earth support, Rowe's method (1952) and Blum's method (1931) are examples of the limit equilibrium approach. Empirical methods are used to obtain prop forces for multi-propped wall systems. Terzaghi and Peck [7] found the most widely used apparent pressure diagrams that provide conservative lateral earth pressure distributions based on field measurements (Fig. 1). Distributed Prop Load (DPL) was created by [8] as a result of enhancing the work of [7] to make it relevant to the UK practice (Table I).

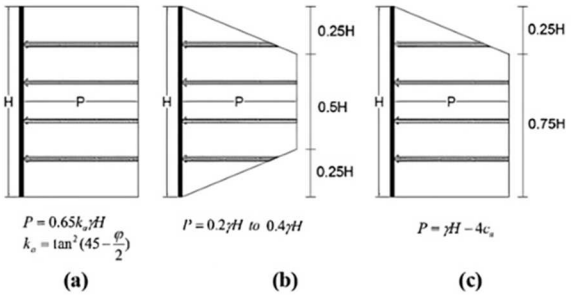

Fig. 1. Apparent earth pressure diagrams introduced by [7]. (a) Sands, (b) Stiff-hard clays, and (c) Soft to medium clay

TABLE I. MATERIAL PROPERTIES OF THE LATERAL SUPPORTS [9]

Class	Soil	Over retained height	DPL
AS	Same as AF for medium strength clay		
AF	Medium strength clay	Top 20%	$0.2\,\gamma H$
		Bottom 80%	$0.3\,\gamma H$
	Low strength clay with stable base	Top 20%	$0.5\,\gamma H$
		Bottom 80%	$0.65\,\gamma H$
	Low strength clay with enhanced base stability	Top 20%	$0.65\,\gamma H$
		Bottom 80%	$1.15\,\gamma H$
BS	High to very high strength clay	All	$0.5\,\gamma H$
BF	High to very high strength clay	All	$0.3\,\gamma H$
C	Granular soil, dry	All	$0.2\,(\gamma - \gamma_w)H$
	Granular soil, submerged	Above water	$0.2\,\gamma H$
		Below water	$0.2\,(\gamma - \gamma_w)\,H + \gamma_w\,(z - d_w)$

All the above methods cannot estimate the wall displacement. Advances in technology have led to the design

979-8-3503-4521-6/23/$31.00©2023 IEEE

of computer software to investigate and analyze the behavior of retaining structures with greater accuracy. Although numerical methods are available, selecting the relevant constitutive model and defining appropriate parameters is difficult in many situations [10]–[12]. Currently, many studies are performed using finite element models for deep excavations. Soil stiffness was found to be the parameter that has the dominant control over excavation-induced ground movement [1], [13], [14]. There are different types of soil stiffness parameters. Some of them are the elastic modulus (E_{50}), the unloading-reloading modulus (E_{ur}), and the initial tangent modulus (E_0), which are presented in Fig. 2.

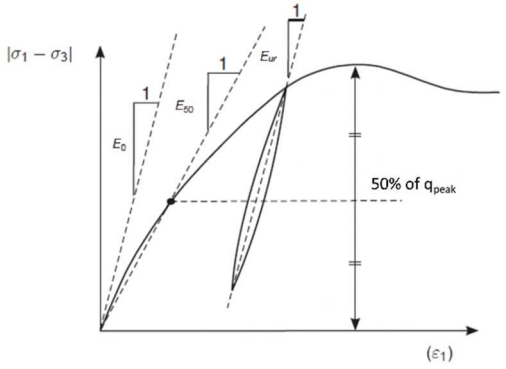

Fig. 2. Definition of E_{50} and E_{ur} in drained triaxial test

In soil unloading problems, such as tunnel construction and excavation, E_{ur} is used instead of E_{50} [15]. E_{ur} is the primary concern in deep excavations because it directly affects the stability of the excavation walls. When a deep excavation is performed, the surrounding soil is subject to changes in stress conditions. As the excavation progresses, the soil around the excavation is unloaded, and the stress condition changes from a state of lateral compression to a state of lateral tension. It can cause the soil to deform and can lead to a reduction in stiffness, making the retaining walls unstable and prone to collapse. Therefore, it is essential to consider the unloading-reloading modulus of soil during the design of deep excavations. There are study outcomes indicating that the elastic modulus (E_{50}) of soil can be increased by several times to obtain the unloading-reloading modulus (E_{ur}) of soil [16], [17].

Most studies have calibrated the models by back-analysis on critical parameters to minimize the deviation between numerically analyzed results and field measurements. Calvello and Finno [18] stated that the inverse analysis methodology effectively calibrates soil parameters. Hardening Soil (HS) and Mohr-Coulomb (MC) models are widely used constitutive models. Khoiri and Ou [19] found that the HS model provides a more accurate fit than the MC model, as it adapts a nonlinear stress-strain curve. Hsiung et al. [3] indicated that reasonably good predictions of the wall displacement could be obtained using the MC model. The availability of field test data for this study was inadequate to use the HS model. Therefore, the linear elastic perfectly plastic MC model was used in this study.

This study proposes a method using two-dimensional analysis to select appropriate parameters and correct modeling procedures in the numerical modeling of deep excavations using measured field data. For that, the horizontal deformation profile of the secant pile wall, the effect of the elastic modulus of soil on the lateral deformation of the wall, the effect of mesh density on the wall deformation, comparison of prop forces using numerical and empirical methods, and the lateral earth pressure distribution near the wall were investigated.

II. Site Description

An excavation performed to construct a hospital complex for the Los Angeles Medical Center Hospital was selected for this study. It is located in a heavily congested area with several multi-story buildings near the site boundary. The hospital building consists of 15 floors, including two basement floor levels. The excavation area has an odd shape with a maximum length and width of 47 and 33 meters, respectively. The typical plan view of the excavation area is presented in Fig. 3. There are two excavation levels at the site. The general excavation of 8.6 m and 10.3 m for areas that locate the lift and services. A 0.88 m thick secant pile with a socketed depth of 0.5 m into the bedrock was used to retain the excavation area during construction. Two lateral support levels support the area excavated to a depth of 8.6 m, and three lateral support levels support a depth of 10.3 m. Each level of the shoring system consists of an effective prop length and a spacing of 4 m. The groundwater table was observed 2 m below the ground level, and the excavation area mainly consisted of residual soil. The ground condition was analyzed using data obtained from four boreholes (Fig. 3). A typical cross-sectional profile of a borehole is presented in Fig. 4.

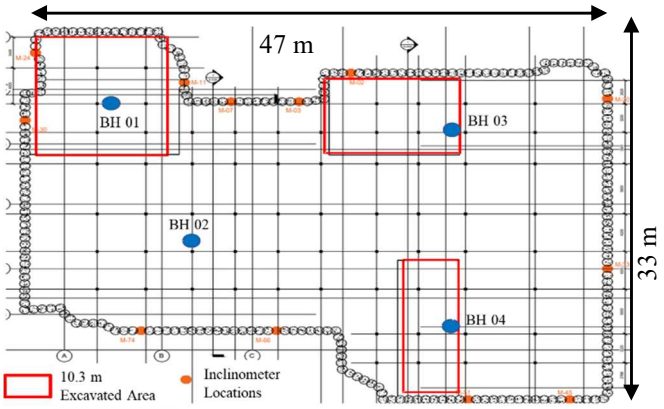

Fig. 3. Excavation area with borehole and inclinometer locations

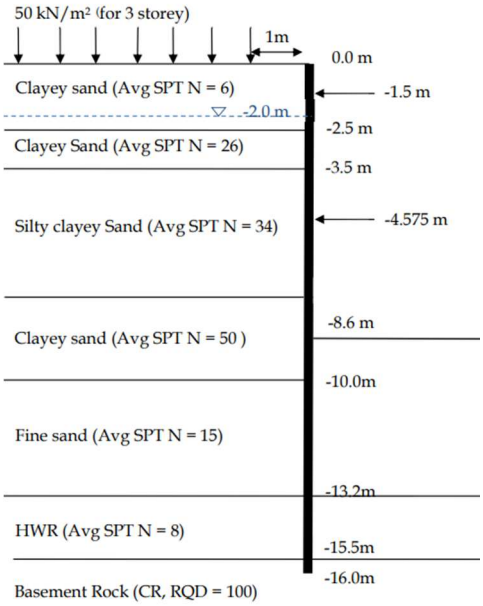

Fig. 4. Subsurface profile of borehole 1

The construction sequences of the two excavation depths are shown in Table II.

TABLE II. CONSTRUCTION SEQUENCE

	8.6 m deep excavation area	10.3 m deep excavation area
Stage 1	Installation of the secant pile wall	Installation of the secant pile wall
Stage 2	Excavate up to -2.0 m elevation	Excavate up to -2.0 m elevation
Stage 3	Installation of first level prop at -1.5 m elevation	Installation of first level prop at -1.5 m elevation
Stage 4	Excavate up to -5.075 m elevation and dewater	Excavate up to -5.075 m elevation and dewater
Stage 5	Installation of second level prop at -4.575 m elevation	Installation of second level prop at -4.575 m elevation
Stage 6	Excavate up to -8.6 m elevation and dewater	Excavate up to -8.4 m elevation and dewater
Stage 7		Installation of third level prop at -7.9 m elevation
Stage 8		Excavate up to -10.3 m elevation and dewater

III. METHODOLOGY

A. Instrumentation

Ground instruments were placed at appropriate locations to monitor the movement of the ground and nearby structures. The monitoring plan included twelve inclinometers placed inside the secant pile wall and two strain gauges placed on the diaphragm wall. The monitoring plan for the project site is illustrated in Fig. 2. The lateral movements of the walls were monitored using a 500 mm long inclinometer torpedo. The readings were taken in the excavation direction at intervals of 0.5 m. Two strain gauges were placed on the retaining wall at a depth of 4.575 m below the ground level.

Measurements were taken once every two weeks according to the monitoring plan to ensure the ground movements were within the acceptable range. The data obtained from the measurements were used to validate the numerical models used in this study. The elastic modulus of the soil was calculated using the SPT N values obtained from the field test data. Eq. (1), introduced by [20] was used to calculate the elastic modulus using the SPT N data. E_b is the modulus of deformation, and N is the standard penetration resistance. Values obtained from the equation were multiplied by two before being used for design work in this project.

$$E_b = 6.78\,N^{0.998} = 7N \quad (1)$$

The friction angle (Ø) was calculated using Eq. (2) extracted from Japanese Railway Standards, which uses the standard penetration resistance for a drill with a standard energy ratio of 70% (N_{70}).

$$\text{Ø} = 0.45\,N_{70} + 20^0 \quad (2)$$

B. Numerical Modeling

PLAXIS 2D finite element software was used in this study. Two-dimensional plane strain triangular mesh elements consisting of fifteen displacement nodes were used to analyze the structure. The boundaries were established twice the maximum excavation depth away from the secant pile wall, and a 25 m thick soil body mesh was used to represent the total thickness of the soil layers. Movements in all directions were restricted at the bottom boundary, and vertical movements were enabled at both vertical boundaries of the model. Soil layers were modeled, and soil properties were assigned according to the borehole data. The excavation area mainly consists of sandy soil. Therefore, an effective stress drained analysis was performed. The dilatancy angle was estimated to be $\varphi = \text{Ø}' - 30^0$ [21] for soils having a friction angle greater than 30^0. The idealized subsurface profile and soil properties based on the borehole data from borehole one are presented in Figs. 4 and 5.

Soil		1 Clayey sand (SPT N = 6)	2 Clayey Sand (SPT N = 26)	3 Silty clayey sand (SPT N = 34)	4 Clayey sand (SPT N = 50)	5 Fine sand (SPT N = 15)	6 HWR (SPT N = 8)
Depth (m)		0.0 to -2.5	-2.5 to –3.5	-3.5 to -7.5	-7.5 to -10.0	-10.0 to -13.2	-13.2 to -15.5
Material Model		Mohr-Coulomb	Mohr-Coulomb	Mohr-Coulomb	Mohr-Coulomb	Mohr-Coulomb	Mohr-Coulomb
γ_{unsat}	[kN/m³]	16.00	20.00	20.00	21.00	17.00	16.00
γ_{sat}	[kN/m³]	17.00	21.00	21.00	22.00	18.00	17.00
k_x	[m/s]	10^{-6}	10^{-6}	10^{-6}	10^{-6}	10^{-4}	10^{-6}
k_y	[m/s]	10^{-6}	10^{-6}	10^{-6}	10^{-6}	10^{-4}	10^{-6}
E_{ref}	[kN/m²]	12000	40000	50000	70000	22000	14000
ν	[-]	0.350	0.300	0.300	0.250	0.300	0.350
c_{ref}	[kN/m²]	3.00	8.00	8.00	10.00	0.00	3.00
φ	[°]	24.00	30.00	32.00	38.00	28.00	25.00
ψ	[°]	0.00	0.00	2.00	8.00	0.00	0.00
$R_{Inter.}$	-	0.67	0.67	0.67	0.67	0.67	0.67

Fig. 5. Soil properties of Borehole 1

The linear elastic material model was used for the secant pile wall and steel struts. One-dimensional fixed-end anchor elements were used as struts in the support system. The Young's modulus and cross-sectional area of struts located at each support level of the shoring system are presented in Table III.

TABLE III. MATERIAL PROPERTIES OF THE LATERAL SUPPORTS

Anchor element	E (GPa)	A (m²)
Prop at -1.5m (200x200x49)	206	$63.53\text{x}10^{-4}$
Prop at -4.575m (300x300x94)	206	$123\text{x}10^{-4}$
Prop at -7.9m (300x300x94)	206	$123\text{x}10^{-4}$

The behavior of the secant pile wall was simplified to a diaphragm wall for the convenience of two-dimensional representation. The retaining wall was modeled using plate elements by idealizing it to a plate element with uniform thickness. Although plate elements have both in-plane and out-of-plane behavior, the out-of-plane behavior was ignored since the plan strain analysis assumes that the wall is infinitely long in that direction. Therefore, only the in-plane deformation should be considered. This is very similar to the actual behavior of a retaining wall. Young's modulus and Poisson's ratio of the wall were set as 31 GPa and 0.2, respectively. Different surcharge values were used in different cases depending on the buildings in the vicinity. 75 kN/m^2 for a five-story building, 50kN/m^2 for a three-story building, and 20 kN/m^2 for a single-story building. The initial groundwater level was defined at 2 m below the ground level. It was kept 0.5 m below the excavation level for all stages within the excavation area to simulate the dewatering process. Steady state pore water pressures were calculated using phreatic conditions assuming that water cannot penetrate into the excavated area beneath the wall since the secant piles were socketed 0.5 m into the bedrock. Medium mesh elements were used for the analysis as recommended by [11]. The mesh was refined close to the retaining wall to increase accuracy. A coarser mesh was used outside the area of interest (Fig. 6).

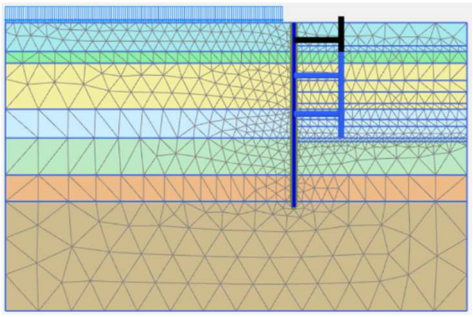

Fig. 6. Mesh distribution

IV. Results and Discussion

A. Horizontal deformation of the secant pile wall with the depth of excavation

It is necessary to validate the model before analysis to ensure it is correct. For validation purposes, the horizontal behavior of the wall was examined with the depth of excavation to determine whether it behaves according to the literature.

Fig. 7 presents the wall movements at different excavation stages of the finite element model created for this study. Under both cantilever and propped conditions at an excavation depth of 2 m, the wall behaved as a cantilever type with similar deformations since the installation of the first prop level initially had little influence. With increasing excavation depth, the behavior of the retaining wall changes from the cantilever type to the braced excavation type under the support system, as mentioned in the literature.

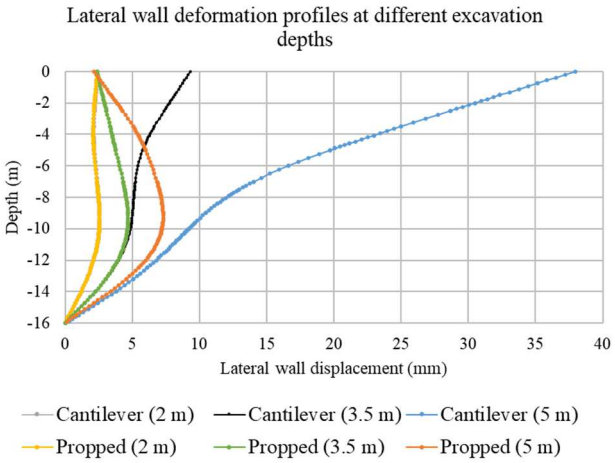

Fig. 7. Lateral wall behavior at different excavation depths

B. Effect of the elastic modulus of soil on the lateral deformation of the wall

The key objective of this study is to conduct a parametric study to increase the elastic modulus of soil used in deep excavation work. The back analysis technique was used to calibrate the elastic modulus of the soil. The M-74, M-66, M-33, and M-51 inclinometer measurements were considered to minimize the corner effect and maintain the plane strain behavior for greater accuracy. Figs. 8 and 9 present the lateral wall deformation profile obtained from the M-66 inclinometer readings compared with the wall deformation profiles obtained from the numerical analysis for different integer multipliers of the elastic modulus of the soil. The distance from the inclinometer to the wall boundary was greater than 5 m to minimize the corner effect [22].

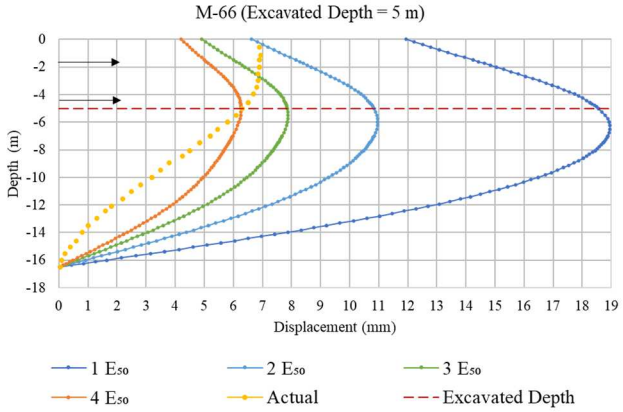

Fig. 8. Comparison of lateral wall deformation at 5 m excavation depth

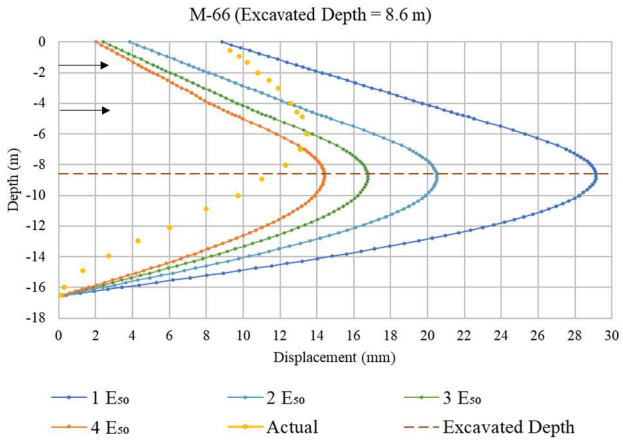

Fig. 9. Comparison of lateral wall deformation at 8.6 m excavation depth

The results indicate that the maximum wall deformation obtained from the inclinometer readings was between the deformation profiles obtained for 2 and 4 times the elastic modulus of the soil at a 5 m excavation depth (Fig. 8). It has been increased to a higher multiple of the elastic modulus of soil with the increase in excavation depth up to 8.6 m (Fig. 9). A similar behavior was observed for the readings of the M-74 inclinometer as well. In both cases, it can be observed that the maximum deflection point has been fitted between higher integer multipliers with the increase in the depth of excavation. According to the literature, the plane strain behavior reduces with increasing excavation depth, where the three-dimensional corner effect reduces the wall deformation from the plane strain behavior. Although the selected inclinometers are located a certain distance from the corner, the lateral deformation of the actual wall underestimates the results obtained from the numerical analysis with increasing excavation depth.

Furthermore, part of the model validation process was performed using field monitoring data. After calibrating the model using the back analysis technique, the maximum deflection point of the actual behavior was between the deformation profiles of 2 – 4 times the elastic modulus of soil at a depth of excavation of 5 m. The maximum deformation of the actual wall is about 40% of the maximum deformation of the profile obtained from the numerical analysis using the

elastic modulus as soil stiffness. This reduction narrows to 35% when 2 E_{50} is used as soil stiffness.

Although the M-33 and M-51 inclinometers were located at acceptable locations, the plotted inclinometer data show cantilever-type wall behavior at higher excavation depths (Fig. 10). It may be caused by insufficient stiffness of struts due to improper fixity of the uppermost lateral supports [23]. Although it has cantilever-type behavior, the maximum deflection was between profiles with higher integer multiples of the elastic modulus of soil, even at a higher excavation depth with the presence of the corner effect.

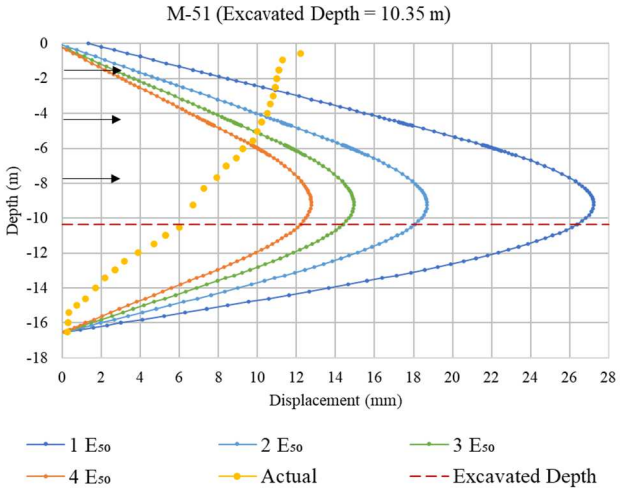

Fig. 10. Comparison of lateral wall deformation at 10.35 m excavation depth

C. *Effect of mesh density on wall deformation*

The lateral wall deformation was checked for medium, fine, and very fine distributions at different excavation depths to verify the influence of mesh distribution on the wall deformation. Fig. 11 represents the numerical analysis results for 2 m and 8.4 m using all three mesh distributions. According to the results obtained from the analysis, no significant deviations were observed at any excavation depth. The percentage of deviation was higher at shallower excavation depths compared to deviations at higher depths due to lower lateral deformation. It becomes negligible when the lateral deformation increases with the increase in excavation depth.

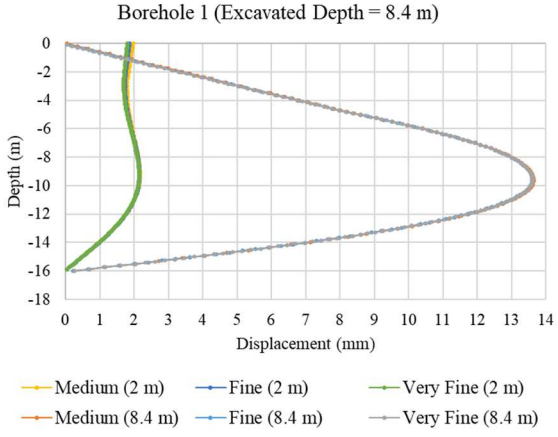

Fig. 11. Lateral wall deformation profiles for different mesh distributions at 2 m and 8.4 m excavation depths

D. *Evaluation of prop forces using numerical and empirical methods*

Prop forces were evaluated using numerical analysis for different excavation depths to compare with different empirical methods for validation. Table IV presents the prop forces obtained from the numerical analysis compared with Terzaghi & Peck and DPL methods, considering the soil as sand and clay separately.

TABLE IV. COMPARISON OF PROP FORCES

Stage	Strut Level	Finite Element Analysis	Peck Method (Sand)	Peck Method (Clay)	DPL Method (Sand)	DPL Method (Clay)
		(kN/m)	(kN)	(kN)	(kN)	(kN)
Stage 5	1	101.77	118.15	119.73	88.16	220.4
Stage 6	1	58.05	148.75	150.8	132.15	330.32
	2	325.79	215.54	318.07	233.96	396.61
Stage 8	1	33.74	164.01	162.04	156.77	391.95
	2	360.89	205.55	330.38	241.63	412.58
	3	308.84	268.73	430.22	260.96	384.21

The prop forces obtained from both methods for sandy soil had higher values for the uppermost strut level and lower prop forces for the second and third strut levels at all stages of excavation. A similar behavior was observed by [24]. One of the critical observations in that study was that the lateral earth pressure of the sand exceeds the pressure obtained from the empirical calculations at higher depths. When the earth pressure of soil obtained from the numerical analysis exceeds the values obtained from the empirical calculations, prop forces become higher on the numerical analysis since they directly influence the forces acting on the support system. Results obtained for clayey soil from both Peck and DPL methods provide results closer to the FE analysis than those obtained for sandy soil for lower strut levels. The DPL method for clay soil provides the highest prop forces out of all.

E. *Evaluation of lateral earth pressure distribution using numerical and empirical methods*

In addition to calculating prop forces, the lateral earth pressure distribution was observed along the wall to verify the values obtained in Section D. Fig. 12 compares the earth pressure distributions obtained from the numerical analysis with the empirical equations used to calculate the strut forces in Section D.

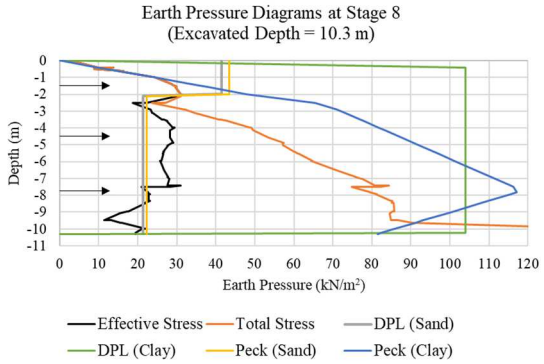

Fig. 12. Comparison of lateral earth pressure distributions

The DPL method for clay soil provides the highest soil earth pressure, creating the most conservative apparent earth pressure diagram. It was the reason for obtaining the highest prop loads in Section D. The Peck method for clay soils has

higher earth pressures than those obtained from numerical analysis. For both Peck and DPL approaches, earth pressures obtained for sandy soil provide lower values below the groundwater level compared to the results of the numerical analysis. It was mainly due to the use of submerged unit weight instead of unsaturated unit weight in earth pressure calculations below the groundwater level, which reduced the unit weight of soil. As a result, lower prop force values were obtained for lower prop levels during the prop load evaluation.

V. Conclusions

The elastic modulus values calculated using the SPT N data can be increased between 2 and 4 times to design retaining structures for deep excavations to obtain an accurate wall behavior with respect to the actual conditions. The lateral deformation was further underestimated with the increase in excavation depth due to corner effects. The influence of the three-dimensional corner effect had a significant effect on the deformation profiles obtained from inclinometer readings near the wall boundary.

The mesh distribution does not have any significant effect on the deformation of the lateral wall and the prop forces. Therefore, a medium mesh can be used in the two-dimensional analysis for deep excavations to reduce the complexity and computational time. The prop forces obtained for both Peck and DPL methods had higher prop forces for the uppermost prop level and lower prop forces for lower prop levels compared to the results of the FE analysis. Reduction in the earth pressure distribution of Peck and DPL methods for sandy soil compared to the results of the FE analysis due to the decrease in the unit weight of the soil below the groundwater level was the main reason for this observation. It was verified by comparing the earth pressure distribution near the retaining wall obtained from the numerical analysis with the same empirical methods.

Acknowledgment

Special thanks to the Department of Civil Engineering at the University of Moratuwa and to the International Construction Consortium (Pvt) Ltd project team that worked on the Los Angeles Medical Center Hospital project for the continuous support of the research.

References

[1] B.-C. B. Hsiung, "A case study on the behaviour of a deep excavation in sand," *Comput. Geotech.*, vol. 36, no. 4, pp. 665–675, 2009, doi: 10.1016/j.compgeo.2008.10.003.

[2] C. Y. Ou, *Deep Excavation: Theory and Practice*. CRC Press, 2006. [Online]. Available: https://books.google.lk/books?id=lgfLrFUdk7EC

[3] B.-C. Hsiung, K.-H. Yang, W. Aila, and C. Hung, "Three-dimensional effects of a deep excavation on wall deflections in loose to medium dense sands," *Comput. Geotech.*, vol. 80, pp. 138–151, 2016, doi: 10.1016/j.compgeo.2016.07.001.

[4] C. A. Coulomb, "Essai Sur Une Application Des Maximis et Minimis a Queques problems Des Statique Relatifsa1‟ Architecture," *Nem. Div. Sav. Acad, Sci*, vol. 7, 1776.

[5] W. J. M. Rankine, "II. On the stability of loose earth," *Philos. Trans. R. Soc. London*, no. 147, pp. 9–27, 1857.

[6] G. Katsigiannis, H. F. Schweiger, P. Ferreira, and R. Fuentes, "Design of Deep Supported Excavations : Comparison Between Numerical and Empirical Methods," in *Geotechnical Safety and Risk V*, 2015, pp. 479–485. doi: 10.3233/978-1-61499-580-7-482.

[7] K. Terzaghi and R. B. Peck, *Soil mechanics in engineering practice (2nd edition)*, Second Edi. New York: John Wiley & Sons, 1967. [Online]. Available: https://books.google.lk/books?id=AnbHzgEACAAJ

[8] D. Twine and H. Roscoe, *Temporary propping of deep excavations-guidance on design, C517*. London: Construction Industry Research and Information Association, 1999. doi: https://doi.org/10.1680/geot.10.P.072.

[9] ArcelorMittal Commercial RPS, *Piling Handbook*, 9th ed. Luxembourg: Imprimerie Centrale, 2016.

[10] B.-C. Hsiung, "Engineering performance of deep excavations in Taipei," University of Bristol, 2002.

[11] S. Likitlersuang, C. Surarak, D. Wanatowski, E. Oh, and A. Balasubramaniam, "Finite element analysis of a deep excavation: A case study from the Bangkok MRT," *Soils Found.*, vol. 53, no. 5, pp. 756–773, 2013, doi: 10.1016/j.sandf.2013.08.013.

[12] M. A. Nikolinakou, A. J. Whittle, S. Savidis, and U. Schran, "Prediction and Interpretation of the Performance of a Deep Excavation in Berlin Sand," *J. Geotech. Geoenvironmental Eng.*, vol. 137, no. 11, pp. 1047–1061, 2011, doi: 10.1061/(asce)gt.1943-5606.0000518.

[13] Y. M. Hou, J. H. Wang, and L. L. Zhang, "Finite-element modeling of a complex deep excavation in Shanghai," *Acta Geotech.*, vol. 4, no. 1, pp. 7–16, 2009, doi: 10.1007/s11440-008-0062-3.

[14] M. I. Ramadan and M. Meguid, "Behavior of cantilever secant pile wall supporting excavation in sandy soil considering pile-pile interaction," *Arab. J. Geosci.*, vol. 13, no. 12, 2020, doi: 10.1007/s12517-020-05483-8.

[15] Bentley Systems, *PLAXIS 2D - Material Models Manual*. 2020.

[16] T. N. Duc, P. Vo, and T. T. Thi, "Determination of unloading—reloading modulus and exponent parameters (m) for hardening soil model of soft soil in ho chi minh city," in *Proceedings of the International Conference on Sustainable Civil Engineering and Architecture 2019*, 2020, vol. 80, no. January, pp. 677–689. doi: 10.1007/978-981-15-5144-4_65.

[17] V. Nguyen and C. Luu, "Influence of unloading soil modulus on horizontal deformation of diaphragm wall," in *Proceeding of international symposium on new technologies for urban safety of mega cities in Asia*, 2013, no. October, pp. 1247–1255.

[18] M. Calvello and R. J. Finno, "Selecting parameters to optimize in model calibration by inverse analysis," *Comput. Geotech.*, vol. 31, no. 5, pp. 410–424, 2004, doi: 10.1016/j.compgeo.2004.03.004.

[19] M. Khoiri and C.-Y. Ou, "Evaluation of deformation parameter for deep excavation in sand through case histories," *Comput. Geotech.*, vol. 47, pp. 57–67, 2013, doi: 10.1016/j.compgeo.2012.06.009.

[20] I. Yoshida and R. Yoshinaka, "A Method to Estimate Modulus of Horizontal Subgrade Reaction For a Pile," *Soils Found.*, vol. 12, no. 3, pp. 1–17, 1972, doi: https://doi.org/10.3208/sandf1972.12.3_1.

[21] M. D. Bolton, "Strength and dilatancy of sands The strength and dilatancy of sands," *Géotechnique*, vol. 36, no. 1, pp. 65–78, 1986, doi: 10.1680/geot.1986.36.1.65.

[22] K. H. Law, Z. Ismail, and R. Hashim, "3D finite element analysis of a deep excavation considering the effect of anisotropic wall stiffness," in *19th Southeast Asian geotechnical conference & 2nd AGSSEA conference (19SEAGC & 2AGSSEA)*, 2016, pp. 659–664. [Online]. Available: https://www.researchgate.net/publication/327867642

[23] A. Osouli and Y. M. A. Hashash, "Case studies of prediction of excavation response using learned excavation performance," *ISSMGE Int. J. Geoengin. Case Hist.*, vol. 1, no. 4, pp. 340–366, 2010.

[24] B. J. S. Chee, "Analysis of strut forces for braced excavations in sand," 2014. [Online]. Available: http://hdl.handle.net/10356/60052